Proc. Natl. Acad. Sci. USA
Vol. 87, pp. 9774–9778, December 1990
Biophysics

Simultaneous monitoring of light-induced changes in protein side-group protonation, chromophore isomerization, and backbone motion of bacteriorhodopsin by time-resolved Fourier-transform infrared spectroscopy

(proton transfer/internal aspartic residues)

KLAUS GERWERT*, GEORG SOUVIGNIER, AND BENNO HESS

Max-Planck-Institut für Ernährungsphysiologie, Rheinlanddamm 201, W-4600 Dortmund 1, Federal Republic of Germany

Communicated by Walther Stoeckenius, September 10, 1990 (received for review June 13, 1990)

ABSTRACT **Absorbance changes in the infrared and visible spectral range were measured in parallel during the photocycle of light-adapted bacteriorhodopsin, which is accompanied by a vectorial proton transfer. A global fit analysis yielded the same rate constants for the chromophore reactions, for protonation changes of protein side groups, and for the backbone motion. From this result we conclude that all reactions in various parts of the protein are synchronized to each other and that no independent cycles exist for different parts. The carbonyl vibration of Asp-85, indicating its protonation, appears with the same rate constant as the Schiff base deprotonation. The carbonyl vibration of Asp-96 disappears, indicating most likely its deprotonation, with the same rate constant as for the Schiff base reprotonation. This result supports the proposed mechanism in which the protonated Schiff base, a deprotonated aspartic acid (Asp-85) on the proton-release pathway, and a protonated aspartic acid (Asp-96) on the proton-uptake pathway act as internal catalytic proton-binding sites.**

Recently, the structure of two membrane proteins, the photosynthetic reaction center and bacteriorhodopsin (bR), have been determined at near-atomic and molecular resolution, respectively (1, 2). In order to understand the structure–function relationship on an atomic level, time-resolving methods have to be applied to yield insight into the intramolecular reactions. Here, the light-driven proton pump bR (3) is investigated by time-resolved Fourier-transform infrared (FTIR) difference spectroscopy (4, 5).

The proton-transfer reactions of bR are initiated by a light-induced isomerization reaction of the chromophore retinal. This reaction is followed by protonation changes of the protonated Schiff base binding site between chromophore and protein and internal aspartic acids of the protein (6, 7). Based on these results, it has been proposed that the interplay between the protonated Schiff base and a deprotonated and a protonated internal aspartic acid describes the principal features of the pump mechanism (5, 6). By using mutant proteins in which internal aspartic acids were altered, these two residues were identified as Asp-85 and Asp-96 by static FTIR difference spectroscopy (8, 9). Substitution of these two residues results in defective proton pumping by the mutated proteins (10, 11).

To determine simultaneously the light-induced kinetics in various parts of the protein, including the protonation changes of Asp-85 and Asp-96 relative to the Schiff base, we performed time-resolved FTIR experiments and, in parallel, measured absorbance changes in the visible spectral range.

The publication costs of this article were defrayed in part by page charge payment. This article must therefore be hereby marked "*advertisement*" in accordance with 18 U.S.C. §1734 solely to indicate this fact.

MATERIALS AND METHODS

Purple membrane was isolated as described (12). Wet, highly concentrated purple membrane pellets in distilled water were squeezed between two CaF_2 windows, separated by a 2.5-μm spacer in a homemade sample chamber. The final OD was $\approx$0.5 and the pH $\approx$6. No salt was added. IR spectra were recorded on a Bruker IFS 88 instrument with the modifications and additional options described earlier (5, 13). Time resolution was about 7 ms (14). The data shown represent a series of four independent measurements. Absorbance changes were recorded simultaneously between 1800 cm^{-1} and 1000 cm^{-1} with 4-cm^{-1} spectral resolution. Absorbance changes in the visible region were measured in parallel at 410, 530, 550, 570, 590, 620, and 660 nm. The apparent rate constants were determined by a global fit analysis (15) on a Convex C2 computer. In addition to the procedure described (15), the differences between the data points and the calculated values for each wavelength were weighted with the estimated noise of the data points. For this estimation we used data taken at the same wavelength before the laser flash (16). As criteria for the fit quality, the improvement of the standard deviation and the residual plots were used (15). Absorbance changes at seven wavelengths in the visible range were taken into account in one calculation. The IR difference spectra were divided in pieces (see Table 1) that were analyzed separately by the global fit procedure. In each piece (Table 1) all absorbance changes with a stepwidth of 2 cm^{-1} were taken into account; e.g., between 1499 cm^{-1} and 1300 cm^{-1} absorbance changes at 100 different wavenumbers were regarded in one fit.

RESULTS

In the proton-pumping photocycle of light-adapted bR, several intermediates with different absorption maxima occur. In order of their appearance in the photocycle they are designated as K, L, M, N, and O (17). In our analysis the light-induced absorbance changes in the visible spectral region of purple membrane suspensions, under the assumption that all follow first-order kinetics, yield the same seven rate constants and corresponding amplitude spectra as found by Xie *et al.* (ref. 15; values given here in parentheses), except for k_1, due to lower time resolution: k_1 = (0.01) ms, k_2 = 0.04 (0.04) ms, k_5 = 0.1 (0.1) ms, k_7 = 0.6 (0.3) ms, k_4 = 2 (2) ms, k_3 = 7 (5) ms, k_6 = 22 (25) ms. The rate constants k_7 and k_6 have small amplitudes and were not observed by Maurer *et al.* (18). To determine absorbance changes in the IR spectral region it is necessary to use thin films instead of suspensions because of the high background absorbance of

Abbreviations: bR, bacteriorhodopsin; FT, Fourier transform.
*To whom reprint requests should be addressed.

Table 1. Time constants (ms)

	Chromophore (410–660 nm)	Side groups (1780–1680 cm^{-1})		Backbone amide I (1671–1650 cm^{-1})		Chromophore backbone (1581–1499 cm^{-1})	Mixed (1499–1300 cm^{-1})	Chromophore (1211–1164 cm^{-1})
k_5	0.6	—		—		—	—	—
k_4	20	25	22	16	22	26	23	27
k_3	73		75		64	71	70	85
		100		113				
k_6	162		155		141	140	133	200

Time constants (ms) for wet purple membrane films were measured at 278 K, in the visible range at 410, 500, 550, 570, 620, and 660 nm and, in parallel, in the IR between 1800 and 1000 cm^{-1}. Due to the lower signal-to-noise ratio, in the region 1780–1680 cm^{-1} the splitting of the 100-ms component into 75-ms and 155-ms components and in the region 1671–1650 cm^{-1} the splitting of the 113-ms component to 64-ms and 141-ms components do not improve the standard deviation and residual plots. However, fits with different sets of start values yield the same result.

water. As a control, the apparent rate constants of such purple membrane films were also determined in the visible range. The absorbance changes of suspensions and films are indistinguishable, in agreement with earlier observations (19), and the global fit analysis yields within the error range the same rate constants and amplitude spectra for both sample preparations.

Because of this 7-ms time resolution for measuring IR absorbance changes by the fast-scan technique (14), the photocycle was slowed by cooling the sample to 278 K (see Table 1). The rate constants follow, within the error range, Arrhenius behavior (ref. 15 and unpublished data) and the corresponding amplitude spectra also show qualitatively the same wavelength dependence as at room temperature (data not shown). As expected, their amplitudes decrease in the red because the apparent O amplitude decreases with decreasing temperature. The rate constant k_7 can no longer be observed and, compared with the results of room temperature, the amplitudes are in general smaller for k_4 and larger for k_6.

Fig. 1 shows IR difference spectra made between spectra recorded before and after initiation of the photocycle with a laser flash. They reflect the M → bR reaction pathway at 278 K. The time dependence of the absorbance changes can be obtained by plotting the amplitudes of the absorbance differences relative to the ground state at a specific wavenumber vs. time as depicted in Fig. 2 *a* and *c* for 1201 cm^{-1} and 1186 cm^{-1}, respectively.

First, the rate constants of absorbance changes in the fingerprint region were determined. As in the visible spectral region these changes are due to reactions of the chromophore. Use of isotopically labeled retinal in resonance-Raman and FTIR experiments has shown that the absorbance bands observed between 1211 cm^{-1} and 1164 cm^{-1} are due to C—C stretching vibrations of the chromophore (for a recent review, see ref. 21). To account for the overlap of absorbance bands of the ground state and the intermediates, the global fit analysis was also applied to the region between 1211 cm^{-1} and 1164 cm^{-1} by using the absorbance data for 24 wavenumbers simultaneously. As expected, within the error range the same rate constants were determined as in the visible spectral range (Table 1).

Fig. 2*a* shows the absorbance change at 1201 cm^{-1} and the fitted curve. The absorbance band at 1201 cm^{-1} mainly represents the C^{14}—C^{15} stretching vibration of all-*trans*-retinal in the light-adapted bR ground state (Fig. 1) (20). The disappearance of the initial bR ground state is not time-resolved. Later in the time course, disappearance of an intermediate also absorbing at 1201 cm^{-1} is indicated by the rate constant k_4. The reappearance of bR is described by the rate constants k_3 and k_6.

The appearance and disappearance of the blue-shifted M intermediate can be followed mainly at 410 nm (Fig. 2*b*). It rises with k_5 (k_2 is not time-resolved) and decays biphasically with k_3 and k_6. The rate constant k_4 has a small contribution to the absorbance change at 410 nm under these measuring conditions (Fig. 2*b*).

The occurrence of an intermediate rising with k_4 after formation of M can be followed at 1186 cm^{-1} (Fig. 2*c*). The absorbance change at 1186 cm^{-1} represents the appearance of a 13-*cis*-retinal configuration with protonated Schiff base, designated as N (22) or L′ (23). Its disappearance can be described by k_3 and k_6.

Appearance and disappearance of the far-red-shifted O intermediate can be followed at 660 nm (Fig. 2*d*). The absorbance change is small compared to the one at 570 nm and at 410 nm because the apparent O amplitude decreases with decreasing temperature. Its appearance is observed with the same rate constant k_4 as the absorbance change at 1186 cm^{-1} rises. Its disappearance follows k_3 and k_6. In the O intermediate, the chromophore has been shown to be all-

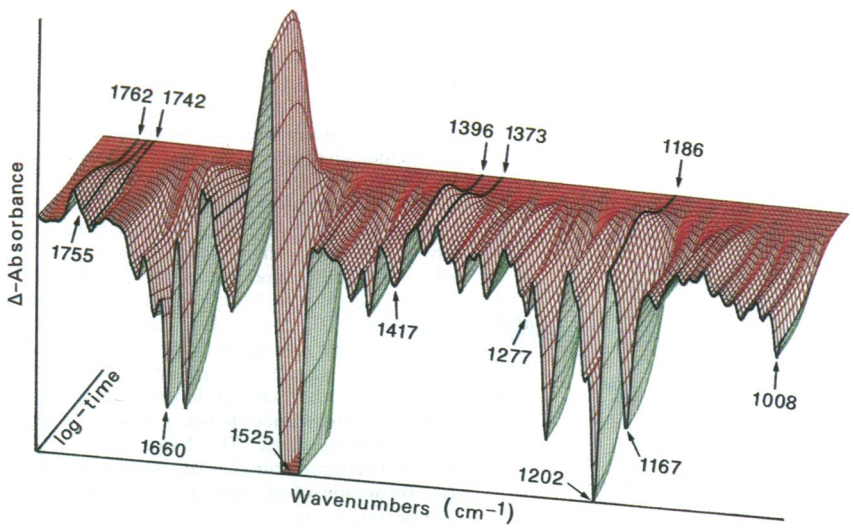

FIG. 1. Light-induced IR absorbance difference spectra between 1800 cm^{-1} and 1000 cm^{-1} of a wet purple membrane film taken at 278 K with the fast-scan FTIR technique with a time resolution of ≈7 ms and spectral resolution of 4 cm^{-1}. The three-dimensional plot shows the fitted curves of the absorbance changes.

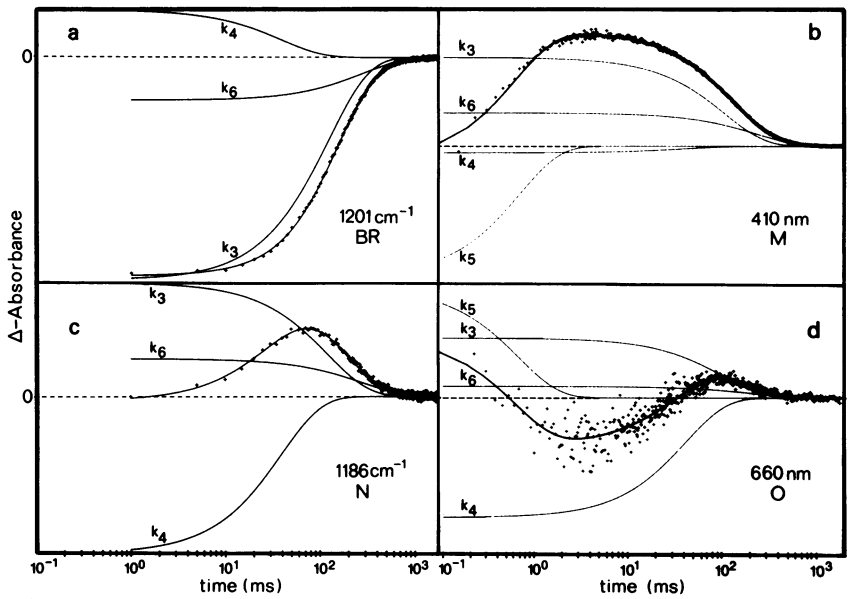

FIG. 2. Light-induced absorbance changes in the IR and visible spectral range, measured in parallel. Absorbance changes (data symbols), the fitted curve (solid line), and the *e*-functions (k_i) of which the fitted curve is composed are shown. (*a*) The absorbance change at 1201 cm^{-1} represents mainly the disappearance of the bR ground state. Its disappearance is not time-resolved below 7 ms. Later on, disappearance of this absorbance band is described by k_4, and reappearance by k_3 and k_6. (*b*) The absorbance change at 410 nm describes mainly the appearance and disappearance of the M intermediate. Its appearance is described by k_5 (k_2 is not time-resolved) and its disappearance by k_3 and k_6. (*c*) The absorbance change at 1186 cm^{-1} describes the appearance of an intermediate with reprotonated Schiff base and 13-*cis*-retinal configuration after formation of M (compare *b*). In a linear scheme it would represent N. Its appearance is described by k_4 and its disappearance by k_3 and k_6. (*d*) The absorbance change at 660 nm describes mainly the appearance and disappearance of the O intermediate. The signal-to-noise ratio is not as good as in *a*–*c* because the apparent O amplitude is decreased at 278 K. However, the global fit analysis yields reliable results because the absorbance changes at the other wavelengths are also regarded. The appearance of O is described by k_4 and its disappearance by k_3 and k_6.

trans-retinal (24). It is remarkable that the 13-*cis* configuration seen at 1186 cm^{-1} and the all-*trans* configuration rise with the same apparent rate constant.

In the following, the kinetics of opsin reactions are compared with those of chromophore reactions.

Above 1650 cm^{-1}, only changes in the opsin part of the molecule are detected. The vibration having the highest possible chromophore frequency, the C=NH$^+$ stretching vibration, is observed at 1643 cm^{-1} in bR and N (22) or L′ (23). Absorbance changes above 1680 cm^{-1} are mostly due to carbonyl vibrations of protein side groups. It was shown that four internal aspartic residues, later assigned to Asp-85, Asp-96, Asp-115 and Asp-212, cause absorbance bands due to protonation and/or hydrogen-bond changes (6–9).

The global fit analysis taking into account all absorbance changes in the carbonyl region between 1780 cm^{-1} and 1680 cm^{-1} shows within the error range the same rate constants as the absorbance changes in the fingerprint and visible spectral region (Table 1). Nevertheless, the biphasic decay by k_3 and k_6 is less significant, due to a smaller signal-to-noise ratio as compared with the fingerprint region.

The appearance of the carbonyl band of Asp-85 at 1764 cm^{-1} and of another internal aspartic acid at 1755 cm^{-1} is shown in Fig. 3 *a* and *c*, respectively; the disappearance of the carbonyl band of Asp-96 at 1741 cm^{-1} is shown in Fig. 3*b* (8, 9). Protonation (deprotonation) of an aspartic acid is indicated by appearance (disappearance) of its carbonyl vibration and hydrogen-bond changes by frequency shifts.

Transient protonation of Asp-85 is not time-resolved (Fig. 3*a*). Its deprotonation is dominated by k_3. It is important to show that Asp-85 is protonated in M (Fig. 2*b*).

The carbonyl vibration of Asp-96 disappears, which was used as indication of its deprotonation (9), with the rate constant k_4, clearly after formation of M (Fig. 2*b*). The same rate constant describes reprotonation of the Schiff base (Fig. 2*c*). Reprotonation of Asp-96 occurs with k_3 and k_6. The absorbance change does not start from the baseline, because Asp-96 first undergoes a hydrogen-bond change in L, which

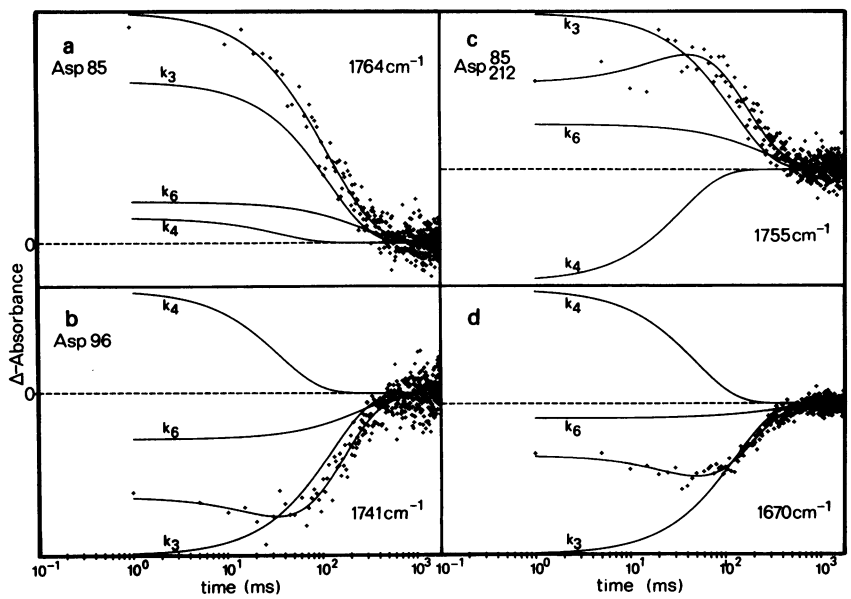

FIG. 3. Absorbance changes in the carbonyl stretching-vibration region. (*a*) Absorbance changes of the carbonyl vibration of Asp-85 at 1764 cm^{-1}. Protonation of Asp-85 is not time-resolved. We have shown earlier that Asp-85, formerly designated Asp-2, is protonated in the L → M transition (6). Reprotonation is mainly described by k_3 and a minor contribution from k_6. (*b*) Absorbance changes of the carbonyl vibration of asp Asp-96 at 1741 cm^{-1}, which indicates most likely its deprotonation (9). Disappearance caused by frequency shifts of the carbonyl vibrations of Asp-96 and Asp-115 are already observed in L due to hydrogen-bond changes (8, 9). The global fit analysis shows an additional disappearance with k_4. Reprotonation can be described by k_3 and k_6. (*c*) Absorbance change at 1755 cm^{-1} indicates protonation of an internal aspartic residue, Asp-85 or Asp-212, with k_4 and its deprotonation with k_3 and k_6. (*d*) Absorbance change at 1670 cm^{-1} in the amide I spectral range. This band indicates most likely a structural motion of the peptide backbone after formation of M with the rate constant k_4. Reappearance can be described by k_3 and k_6.

leads to a large negative band at 1741 cm^{-1} at earlier times (6). In ref. 8 this was interpreted as deprotonation of Asp-96 in L. But deprotonation seems unlikely, because no corresponding carboxylate vibration of Asp-96 was observed in L (9). The global fit analysis shows now clearly an additional absorbance decrease at 1741 cm^{-1} with the rate constant k_4. At higher pH, at which the N intermediate is more accumulated, this band is strongly increased; at lower pH its intensity is decreased due to lower N contribution (G.S. and K.G., unpublished data). The conclusion that Asp-96 is deprotonated is supported by the observation that the absorbance change at 1378 cm^{-1}, which was tentatively assigned at least partially to the corresponding carboxylate vibration, appears also with the rate constant k_4. The absorbance change at 1755 cm^{-1} indicates the protonation of an internal aspartic residue—Asp-85 or Asp-212 (9)—clearly after formation of M, with the rate constant k_4 and deprotonation of this residue with k_3 (Fig. 3*c*).

Above 1770 cm^{-1} a continuum absorbance decrease is seen (data not shown). Under the measuring conditions used, this absorbance change is much smaller than at 1741 cm^{-1}.

Reactions of the protein backbone should be reflected by absorbance changes around 1655 cm^{-1}, at which the amide I vibration is observed. Difference bands in this region were assigned to a structural change of the protein backbone (4, 9, 25). To determine the kinetics of these absorbance changes the global fit analysis was applied to the region between 1650 cm^{-1} and 1671 cm^{-1}. Within the error range the same rate constants were yielded for absorbance changes in the amide I spectral region as for the fingerprint region and visible range (Table 1). As an example, an absorbance change at 1670 cm^{-1} is shown in Fig. 3*d*. This absorbance change reflects most likely a shift of an amide I vibration, indicating thereby a structural motion of the protein backbone. This change appears with k_4 and disappears with k_3 and k_6.

The spectral region 1581 cm^{-1} to 1499 cm^{-1}, at which the amide II band absorbs, shows also strong ethylenic bands of retinal (20). The global fit analysis yields for absorbance changes between 1581 cm^{-1} and 1499 cm^{-1} the same rate constants (Table 1).

Chromophore, protein backbone, and protein side-group reactions are detected in the region between 1499 cm^{-1} and 1300 cm^{-1}. But in contrast to the other parts of the difference spectrum, chromophore vibrations show no stronger absorbance bands than the opsin vibrations. The global fit analysis yields again the same rate constants as above (Table 1). Some of the absorbance changes between 1455 cm^{-1} and 1406 cm^{-1} are caused by a light-induced twist around an Xaa-Pro amide bond (26, 27). This structural motion can also be described by the same rate constants. Also, the absorbance change of Tyr-185 at 1277 cm^{-1} follows these rate constants (40).

DISCUSSION

The rate constants for absorbance changes in the visible spectral range and between 1211 cm^{-1} and 1164 cm^{-1} in the IR region are in good agreement (Table 1). This is expected because both absorbance changes reflect chromophore reactions. The agreement verifies the capacity of the applied fast-scan FTIR method to record time-resolved complete difference spectra with 7-ms time resolution (14).

Rate constants for absorbance changes in the IR difference spectra that are caused mainly by protein side-group reactions and protein backbone motions agree with those for the chromophore (Table 1). From this result we conclude that proton pumping is performed by synchronized reactions of the participating groups. Independent cycles for the chromophore and the proton-transfer reactions or structural changes of the backbone can be excluded.

The experimentally determined apparent rate constants are not directly related to natural rate constants because forward reactions alone cannot describe the photocycle (for recent literature, see ref. 28). In principle, the proton-pumping photocycle can be divided into two parts: the reaction pathway from bR to M, in which M rises in the microsecond time range, and the reaction pathway from M to bR, in the millisecond time range. In the first part, protons are released to the extracellular side; in the second, protons are taken up from the cytoplasmic side (17, 29, 30). M seems to be the crucial intermediate at which the central proton-binding site, the protonated Schiff base, is transiently deprotonated. In principle, two different models of the photocycle and their combinations are discussed: (*i*) linear scheme close to the original proposed one (17), in which back-reactions are included between the different intermediates; every symbol could represent more than one species ($K = K_1, K_2, \ldots$; $L = L_1, L_2, \ldots$) (22, 28, 31, 32); (*ii*) at least two parallel photocycles of slightly different bR molecules (23, 28, 33–35). The present results cannot unequivocally distinguish between the two proposed models.

The following conclusions based on simulations with different photocycle models (K.G. and G.S., unpublished results) can be given.

(*i*) The main apparent rate constant that describes the rise of N, followed at 1186 cm^{-1}, has no large contribution under the measuring conditions to the decay of M followed by 410 nm. This can be explained by parallel photocycles. Alternatively, in a linear photocycle scheme, this can be caused by $M \rightarrow L$ and $N \rightarrow M$ back-reactions or by two consecutive M intermediates, M_1 and M_2. An $M_1 \rightarrow M_2$ transition has been proposed (25, 28, 31). Interestingly, the bR − M difference spectrum measured at 200 K differs from the one taken at 270 K in the amide I spectral region at 1670 cm^{-1} and 1650 cm^{-1} (25). This could indicate a structural motion of the backbone during an $M_1 \rightarrow M_2$ transition (4, 26, 27) which is blocked at 200 K. Also relaxation of the light-induced C^{14}—C^{15} single-bond twist of retinal could take place (20, 36).

(*ii*) The O intermediate rises with k_4. This gives further evidence for a fast $N \rightleftharpoons O$ equilibrium (30) in a linear scheme.

(*iii*) The decay of M, N, and O is described by the same rate constants, k_3 and k_6. This points to significant $N \rightarrow M$ and $O \rightarrow N$ back-reactions in a linear scheme.

(*iv*) In the model calculations, k_6 could not be fitted within a linear scheme. This points to a branching reaction, at least after formation of M (28), or, alternatively, to parallel photocycles.

In summary, simulations with a photocycle model (model B) proposed in ref. 28 lead to reasonable agreement between calculated curves and observed data. Nevertheless, parallel photocycles can also explain the data.

How are the protonation changes of the internal aspartic acids related to the photocycle kinetics? Asp-85, formerly designated Asp-2, is protonated in the $L \rightarrow M$ transition (6) (Fig. 4). Therefore, it was proposed to be the proton acceptor for the protonated Schiff base (8–11). Nevertheless, other groups must be involved in the proton-release pathway, because the proton is released from the protein in the $L \rightarrow M$ transition (29, 30), while Asp-85 remains protonated in M (compare Fig. 2*b* and Fig. 3*a*). In the structural model, Asp-85 is positioned close to the Schiff base and, together with Arg-82, is proposed to be on a proton-release pathway (2, 8).

Disappearance of the carbonyl vibration of Asp-96, indicating most likely its deprotonation, is described by k_4 after formation of M. Because reprotonation of the Schiff base, indicated by appearance of a positive band at 1186 cm^{-1}, follows the same kinetics, Asp-96 is very likely the proton donor to the Schiff base, in agreement with earlier proposals (compare Fig. 2*c* and Fig. 3*b*) (9–11, 37, 38). The novelty here

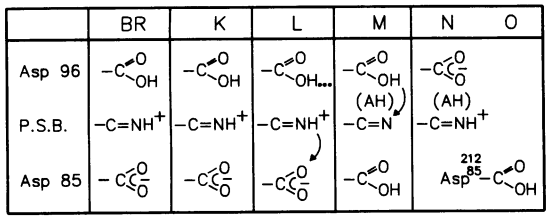

FIG. 4. Protonation changes of Asp-85, Asp-96, and the protonated Schiff base (P.S.B.) during the photocycle. Asp-96 undergoes a hydrogen-bond change in L and is most likely deprotonated with the same apparent rate constant as the Schiff base is reprotonated. This change seems to be the rate-limiting step; however, other groups (AH) undergoing faster protonation changes (e.g., bound water) might be also involved in this reprotonation step. Asp-96 is reprotonated from the cytoplasmic side. Asp-85 is protonated in the L → M transition with the same apparent rate constant as the Schiff base is deprotonated. Another group (e.g., Arg-82) must be involved in the proton-release pathway because a proton is ejected in the L → M transition to the exterior. The carbonyl vibration at 1755 cm^{-1} indicates protonation of an internal aspartic acid, Asp-85 or Asp-212, in O.

is that the protonation kinetics of both involved groups can be resolved and are simultaneously measured. Other groups undergoing faster (here not time-resolved) protonation changes could be involved in the proton transfer between Asp-96 and the Schiff base (9). A collective proton transfer—e.g., via bound water—may be indicated by a transient continuum absorbance decrease above 1770 cm^{-1} during the photocycle. Model compounds have shown that hydrogen-bond chains with large proton polarizability cause continuum absorbance in the IR (39). The structural model suggests an involvement of other groups in the proton transfer between Asp-96 and the Schiff base (2).

Another internal aspartic acid (Asp-212 or Asp-85) is protonated with k_4 in the time range of the O intermediate. If one linear photocycle is assumed, this residue is probably Asp-212, because Asp-85 is already assigned to 1764 cm^{-1} (9). On the other hand, if this band belongs to Asp-85, two parallel cycles have to be assumed. Protonation of this aspartic acid could explain the far-red shift of the O intermediate, because the chromophore charge is not stabilized by a counterion.

It has been demonstrated that by FTIR spectroscopy the intramolecular reactions in different parts of a protein can simultaneously be monitored, time-resolved, at a molecular level.

We thank K. H. Müller for providing us with the excellent global fit program, Dr. G. Varo and Dr. J. Lanyi for very helpful discussions on the photocycle, Dr. D. Bashford and S. Buchanan for correction of the English language, M. Schubert and R. Eichas-Nell for excellent and engaged technical help, Dr. B. Zubov for help during his short visit in an early stage, and Prof. W. Stoeckenius for very useful comments on the manuscript. K.G. acknowledges a Heisenberg Fellowship from the Deutsche Forschungsgemeinschaft.

1. Deisenhofer, J., Epp, O., Miki, K., Huber, R. & Michel, H. (1985) *Nature (London)* **318,** 618–624.
2. Henderson, R., Baldwin, J. M., Ceska, T. A., Zemlin, F., Beckmann, E. & Downing, K. H. (1990) *J. Mol. Biol.* **213,** 899–929.
3. Oesterhelt, D. & Stoeckenius, W. (1973) *Proc. Natl. Acad. Sci. USA* **70,** 2853–2857.
4. Braiman, M. S., Ahl, P. L. & Rothschild, K. J. (1987) *Proc. Natl. Acad. Sci. USA* **84,** 5221–5225.
5. Gerwert, K. & Hess, B. (1988) in *The Ion Pumps: Structure, Function, and Regulation*, ed. Stein, P. (Liss, New York), pp. 321–326.
6. Engelhard, M., Gerwert, K., Hess, B., Kreutz, W. & Siebert, F. (1985) *Biochemistry* **24,** 400–407.
7. Eisenstein, L., Lin, S.-L., Dollinger, G., Odashima, K., Termini, J., Konno, K., Ding, W.-D. & Nakanishi, K. (1987) *J. Am Chem. Soc.* **109,** 6860–6862.
8. Braiman, M. S., Mogi, T., Marti, T., Stern, L. J., Khorana, H. G. & Rothschild, K. J. (1988) *Biochemistry* **27,** 8516–8520.
9. Gerwert, K., Hess, B., Soppa, J. & Oesterhelt, D. (1989) *Proc. Natl. Acad. Sci. USA* **86,** 4943–4947.
10. Butt, H. J., Fendler, K., Bamberg, E., Tittor, J. & Oesterhelt, D. (1989) *EMBO J.* **8,** 1657–1663.
11. Holz, M., Drachev, L. A., Mogi, T., Otto, H., Kaulen, A. D., Heyn, M. P., Skulachev, V. P. & Khorana, H. G. (1989) *Proc. Natl. Acad. Sci. USA* **86,** 2167–2171.
12. Oesterhelt, D. & Stoeckenius, W. (1974) *Methods Enzymol.* **31,** 667–678.
13. Gerwert, K. (1988) *Ber. Bunsenges. Phys. Chem.* **92,** 978–982.
14. Gerwert, K., Souvignier, G. & Hess, B. (1989) *Proc. 7th Int. Conf. FTIR Spectros.* **1145,** 130.
15. Xie, A. H., Nagle, J. F. & Lozier, R. H. (1987) *Biophys. J.* **51,** 627–635.
16. Müller, K. H. & Plesser, Th. (1991) *Eur. Biophys. J.*, in press.
17. Lozier, R., Bogomolni, R. A. & Stoeckenius, W. (1975) *Biophys. J.* **15,** 955–962.
18. Maurer, R., Vogel, J. & Schneider, S. (1987) *Photochem. Photobiol.* **46,** 247–253, 255–262.
19. Korenstein, R. & Hess, B. (1977) *Nature (London)* **270,** 184–186.
20. Gerwert, K. & Siebert, F. (1986) *EMBO J.* **5,** 805–811.
21. Kitagawa, T. & Maeda, A. (1989) *Photochem. Photobiol.* **50,** 883–894.
22. Fodor, S. P. A., Ames, J. B., Gebhard, R., van der Berg, E. M. M., Stoeckenius, W., Lugtenburg, J. & Mathies, R. (1988) *Biochemistry* **27,** 7097–7101.
23. Diller, R. & Stockburger, M. (1988) *Biochemistry* **27,** 7641–7651.
24. Smith, S. O., Pardoen, J. A., Mulder, P. P. J., Curry, B., Lugtenburg, J. & Mathies, R. (1983) *Biochemistry* **22,** 6141–6148.
25. Gerwert, K., Rodriguez-Gonzales, R. & Siebert, F. (1985) *Time-Resolved Vibrational Spectroscopy*, eds. Lauberau, A. & Stockburger, M. (Springer, Berlin), pp. 263–268.
26. Gerwert, K., Hess, B. & Engelhard, M. (1990) *FEBS Lett.* **261,** 449–454.
27. Rothschild, K. J., He, Y. W., Gray, D., Roepe, P., Pelltien, S. L., Brown, R. S. & Herzfeld, J. (1989) *Proc. Natl. Acad. Sci. USA* **86,** 9832–9835.
28. Váró, G. & Lanyi, L. (1990) *Biochemistry* **29,** 2241–2250.
29. Drachev, L. A., Kaulen, A. D. & Skulachev, V. P. (1984) *FEBS Lett.* **178,** 331–335.
30. Grzesiek, S. & Dencher, N. A. (1986) *FEBS Lett.* **208,** 337–342.
31. Kouyama, T., Kouyama, A. N., Ikegami, A., Mathew, M. K. & Stoeckenius, W. (1988) *Biophys. J.* **15,** 955–962.
32. Chernavskii, D. S., Chizhov, I. V., Lozier, R. H., Murina, T. M., Prokhorov, A. M. & Zubov, B. V. (1989) *Photochem. Photobiol.* **49,** 649–653.
33. Korenstein, R., Hess, B. & Kuschmitz, D. (1978) *FEBS Lett.* **93,** 266–270.
34. Hamamoto, J. H., Dupuis, P. & El Sayed, M. A. (1984) *Proc. Natl. Acad. Sci. USA* **81,** 7083–7087.
35. Dancsházy, Zs., Govindjee, R. & Ebrey, T. G. (1988) *Proc. Natl. Acad. Sci. USA* **85,** 6358–6361.
36. Fahmy, K., Grossjean, M. F., Siebert, F. & Tavan, P. (1989) *J. Mol. Struct.* **214,** 257–288.
37. Tittor, J., Soell, Ch., Oesterhelt, D., Butt, H.-J. & Bamberg, E. (1989) *EMBO J.* **8,** 3477–3482.
38. Otto, H., Marti, T., Holz, M., Mogi, T., Lindau, M., Khorana, H. G. & Heyn, M. P. (1989) *Proc. Natl. Acad. Sci. USA* **86,** 9228–9232.
39. Zundel, G. (1988) *J. Mol. Struct.* **177,** 43–68.
40. Braiman, M. S., Mogi, T., Stern, C. J., Hackett, N. R., Chao, B. H., Khorana, H. G. & Rothschild, K. J. (1988) *Proteins* **3,** 219–229.